Carbohydrate Polymers 92 (2013) 555–563

Contents lists available at SciVerse ScienceDirect

Carbohydrate Polymers

journal homepage: www.elsevier.com/locate/carbpol

Amylose-directed synthesis of CuS composite nanowires and microspheres

Yinhui Li [a], Jiwen Hu [a,*], Guojun Liu [a,b,**], Ganwei Zhang [a], Hailiang Zou [a], Jinheng Shi [a]

[a] Guangzhou Institute of Chemistry, Chinese Academy of Sciences, Guangzhou 510650, PR China
[b] Department of Chemistry, Queen's University, 90 Bader Lane, Kingston, Ontario, Canada K7L 3N6

ARTICLE INFO

Article history:
Received 26 March 2012
Received in revised form 15 August 2012
Accepted 26 August 2012
Available online 2 September 2012

Keywords:
Amylose
CuS
Composite particles
Microspheres and nanowires

ABSTRACT

Reported are the synthesis and characterization of CuS composite nanowires and microspheres in the presence of amylose. The preparation involved first the complexation of amylose with Cu^{2+} of $CuCl_2$ at 70 °C. Cu^{2+} complexation was confirmed by a conductivity reduction of $CuCl_2$ after amylose addition. Also, the aggregation state of the amylose changed after Cu^{2+} as revealed by transmission electron microscopy (TEM) and dynamic light scattering (DLS). At the Cu^{2+} to α-D-glucopyranosyl unit molar ratio *r* of 0.70 and 1.41, the amylose aggregated into microspheres that were approximately 150 and 250 nm in diameter. Adding sodium thiosulfate resulted in the production of an amorphous precipitate consisting presumably of CuS_2O_3. At $r = 0.70$ and 1.41, CuS_2O_3 precipitated inside the template of Cu^{2+}/amylose microspheres as nanoparticles, while a twisted nanowire-like structure was produced at $r = 0.92$. CuS_2O_3 decomposed under heating at 100 °C to yield crystalline CuS nanoparticles.

© 2012 Elsevier Ltd. All rights reserved.

1. Introduction

Nanocrystalline copper sulfide is a *p*-type semiconductor which regularly exhibits at least five stable phases with different Cu:S molar ratios. These phases include covellite (CuS), anilite ($Cu_{1.75}S$), digenite ($Cu_{1.8}S$), djurlite ($Cu_{1.95}S$), and chalcocite (Cu_2S) (Lindroos, Arnold, & Leskela, 2000). These materials have been of interest due to their potential applications in nanometer-scale switches (Sakamoto et al., 2003), solar cells (Burton & Windawi, 1976; Hall, Birkmire, Phillips, & Meakin, 1981; Yuan et al., 2008), gas sensors (Yu, Wang, Chan, & Cao, 2009), and lithium rechargeable batteries (Chung & Sohn, 2002). Among these semiconductors with different phases, covellite (CuS) has unique conductive and optical properties, which make it especially suitable for conductive materials (Johansson, Kostamo, Karppinen, & Niinistö, 2002; Liufu, Chen, Yao, & Huang, 2008; Nair, Cardoso, Daza, & Nair, 2001), optical materials (Gao et al., 2008; Zhang & Zhang, 2008), solar cells and sensors (Lee, Yoon, Kim, & Park, 2007), and also as alternative materials for cathodes of lithium rechargeable batteries (Nagarathinam, Chen, & Vittal, 2009). Moreover, covellite (CuS) can be used as a superconductive material due to holes in its valence band, which are associated with the 3p orbitals of sulfur (Buckel & Hilsch, 1950; Folmer & Jellinek, 1980; Liang & Whangbo, 1993; Nozaki, Shibata, & Ohhashi, 1991; Westrum, Stolen, & Gronvold, 1987).

For all of the above-mentioned applications, covellite (CuS) needs to be produced with a certain morphology and size (Hu & Nair, 1996). Because of this, various methods have been developed to synthesize covellite nanocrystals with different architectures, which have included nanodisks (Saunders, Ghezelbash, Smilgies, Sigman, & Korgel, 2006), nanorods (Roy, Mondal, & Srivastava, 2008), nanofibers (Chen, Deng, et al., 2008; Chen, Chen, & Wu, 2008), nanoplates (Xu, Wang, & Zhu, 2006), nanotubes (Mao et al., 2009), flower-like structures (Shen, Zhao, Shu, Zhou, & Yuan, 2009), hollow microspheres (Zhu, Wang, & Wu, 2009) and hierarchical microspheres (Li, Wu, Qin, Li, & Huang, 2010). The preparation of CuS microspheres with hierarchical structures and 1-D CuS nanowires/fibers is of particular importance in theoretical and materials science (Basu et al., 2010; Liu & Xue, 2010; Nagarathinam, Chen, et al., 2009; Nagarathinam, Saravanan, Leong, Balaya, & Vittal, 2009; Wang, Xu, Zou, Luo, & Ying, 2008; Xu & Ding, 2008; Xu, Wang, Cheng, Meng, & Jiao, 2010). So far, there are only a few reports on the formation of covellite (CuS) microspheres with hierarchical structures and 1-D CuS nanowires/fibers. For example, Xie and coworkers (Li, Xie, & Xue, 2007) took advantage of the complex formation between L-cysteine with $CuCl_2$ and assembled them into aggregated spheres. The as-formed precursors were then decomposed as self-sacrifice templates under the hydrothermal condition to produce interesting hierarchical CuS microspheres. Wu and coworkers (Chen, Deng, et al., 2008; Chen, Chen, et al., 2008) synthesized hexagonal CuS particles through the thermolysis of a $Cu(R_2dtc)_2$ (R = octyl, dtc = dithiocarbamate) precursor at 130–180 °C under N_2 flow. The microspheres have an average diameter of 1.74 μm. In addition, Lu and coworkers (Xue et al., 2004) reported the preparation of helical CuS nanofibers with a

* Corresponding author. Tel.: +86 20 85232307; fax: +86 20 85232136.
** Corresponding author. Tel.: +86 20 85232307; fax: +86 20 85232136.
E-mail address: hjw@gic.ac.cn (J. Hu).

0144-8617/$ – see front matter © 2012 Elsevier Ltd. All rights reserved.
http://dx.doi.org/10.1016/j.carbpol.2012.08.102

pitch of 100–200 nm in butyl acetate and benzene–butanol gel systems using cholesterol organogelator as template. The CuS fibers with straight and bending helical structures were obtained by adjusting to sulfur source and/or the organogel systems.

Amylose, the linear soluble portion of starch consisting of (1 → 4)-linked α-D-glucopyranosyl units, is a polysaccharide which is abundant, inexpensive and biocompatible (Cuevas, Gilbert, & Fitzgerald, 2010; Ortega-Ojeda, Larsson, & Eliasson, 2004). Although many reports concern the abrication of functional materials with novel structures using amylose as template or stabilizer (Chairam, Poolperm, & Somsook, 2009; Chang, Yu, Ma, & Anderson, 2011; Vigneshwaran, Nachane, Balasubramanya, & Varadarajan, 2006), to the best of our knowledge, the formation of CuS nanowires and microspheres using amylose as an in situ formed template has not been reported.

In this paper, we report the synthesis of CuS and amylose composite nanowires and microspheres, which are denoted as CuS@amylose particles thereon, using a very simple procedure. That is, Cu^{2+} initially complexed with hydroxyl groups in amylose, which induced amylose aggregation into nano- and micro-particles, $Na_2S_2O_3$ was then added to form CuS_2O_3 precipitates inside the original Cu^{2+}/amylose aggregates, CuS nanowires and microspheres were eventually formed due to a disproportionation reaction of CuS_2O_3 under heating. Since the microspheres seemed to form from many fused CuS@amylose nanoparticles, they can be viewed as a type of hierarchical structure, while CuS@amylose nanowires were obviously 1-D novel structures.

2. Experimental

2.1. Materials and reagents

Amylose [$(C_6H_{10}O_5)_n$, Tianjin Ruijinte Chemical Reagent Co. Ltd., China], copper chloride ($CuCl_2{\cdot}2H_2O$, +97%, Tianjin Keoumi Chemical Reagent Co.), and sodium thiosulfate pentahydrate ($Na_2S_2O_3{\cdot}5H_2O$, +99%, Guangzhou Chemical Reagent Factory) were used as received. Water was doubly distilled with a home-built water purification system.

The amylose stock solution was prepared by magnetically stirring distilled water (99.75 g) and amylose (0.2546 g) in a 200-mL round-bottom flask at 100 ± 1 °C for 30 min to yield a transparent solution. The resultant transparent 0.25 wt% solution was stored at room temperature and was heated to 70 °C before use.

2.2. Size exclusion chromatography

The size exclusion chromatograph consisted of a Waters 515 pump, a Waters 410 differential refractive index detector, and an ultra-Hydrogel® 250 column. The system was calibrated by poly(ethylene glycol) standards and operated at 40 °C. The mobile phase consisted of a 0.1-M aqueous NaCl solution flowing at 0.60 mL/min. The amylose solution was freshly heated to 70 °C before injection.

2.3. Conductivity measurements

To 9.2 mL of the amylose stock solution was added 0.026, 0.20, or 0.40 mL of the 0.50-M $CuCl_2$ solution. Appropriate amounts of distilled water were then added into the first two flasks so that the final volume was 9.6 mL for all three samples. Each of the prepared solutions was divided into two portions. One portion was equilibrated at 28 ± 5 °C (room temperature) for half an hour before conductivity measurement. The other portion was heated to 70 °C for half an hour and then allowed 120 min for the sample to cool to room temperature for conductivity measurement. Conductivity σ was measured on a DDS-11A digital conductometer at 28 ± 5 °C. Also measured were the conductivities σ_0 of three reference samples that were prepared under otherwise identical conditions as mentioned above except the replacement of the amylose stock solution by distilled water.

2.4. CuS@amylose synthesis

The first step toward CuS synthesis involved the preparation of amylose/Cu^{2+} complexes. To 18.4 mL of the 0.25 wt% amylose solution was added dropwise 0.052, 0.40, or 0.80 mL of a 0.50-M aqueous $CuCl_2$ solution. The resultant mixtures at the Cu^{2+} to glucose molar ratio r of 0.092, 0.70, and 1.41 were then stirred at 70 ± 1 °C for 30 min.

Subsequently, 0.077, 0.60, and 1.20 mL of an aqueous 0.50-M $Na_2S_2O_3$ aqueous solution was added under stirring into this solution at 70 ± 1 °C. Within 3 min, the resulting mixture turned light brown. It turned dark brown in 0.5 h and eventually turned black after 2 h in agreement with observations reported in literature (Yamamoto, Tanaka, Kubota, & Osakada, 1993). Following Nagarathinam, Chen, et al. (2009) and Nagarathinam, Saravanan, et al. (2009), each mixture was then transferred into a 30-mL Teflon-lined stainless steel autoclave, sealed, and heated at 100 ± 1 °C for 24 h to yield a black precipitate. The crude product was sequentially washed with ethanol, a poor solvent for amylose, and distilled water each for several times, and freeze-dried under vacuum at −56 °C for 24 h.

For comparison purposes, CuS was also prepared under otherwise identical conditions except that the amylose solution was replaced by water.

2.5. X-ray diffraction study

CuS@amylose powders were placed in a 1.5-cm circular well in a glass plate and were then pressed and compacted by pressing a steel plate on them. X-ray diffraction (XRD) analysis of CuS@amylose was conducted using a Rigaku-Dmax 2400 diffractometer equipped with a graphite monochromatized Cu K_α radiation source (λ = 1.54 Å). The acceleration voltage was set to 50 kV, with 100 mA flux at a scanning rate of 0.02°/s in the 2θ range of 5–80° for measuring wide-angle diffraction patterns.

2.6. UV–visible absorption analysis

CuS@amylose samples were ultrasonicated in doubly distilled water at 1.0 mg/mL for 30 min to generate black suspensions. These suspensions were diluted for UV–visible absorption analysis. The spectra were recorded on a UV-8000 instrument (Shanghai Metash Instruments Company) in the wavelength range of 300–1000 nm.

2.7. Transmission electron microscopy measurements

Transmission electron microscopy (TEM) analyses were performed using a JEM-100CX microscope operated at 80 kV. The Cu^{2+}/amylose complex solutions were aero-sprayed onto Formvar-coated copper grids using a home-built device (Ding & Liu, 1999) dried under ambient conditions for 2 h, and then directly used for TEM observations. The CuS@amylose samples were ultrasonicated before aero-spraying. An amylase solution heated to 70 °C and then cooled room temperature was aero-sprayed analogously. To stain this sample, a drop 2 wt% uranyl acetate solution in water was placed on a sprayed and dried sample for 3 min before the liquid was wicked off using filter paper.

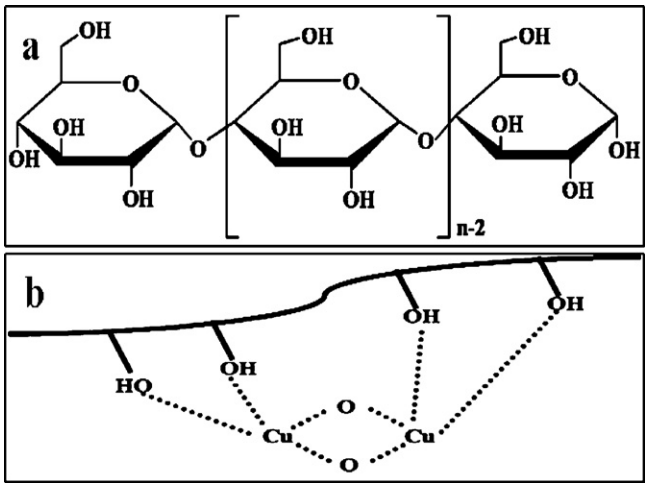

Scheme 1. (a) Primary structure of amylose and (b) Complex formation between PVA and Cu^{2+}.

2.8. Scanning electron microscopic analyses

For scanning electron microscopy (SEM) analysis, droplets of a CuS@amylose suspension were deposited onto a 2 mm × 4 mm polished disk. The disk was then mounted onto an aluminum flat-holder and air-dried at room temperature for 24 h. Subsequently, a thin layer of Au was sputtered onto the sample using by JFC-1600 autofine coater. Scanning electron microcopy (SEM) analyses were performed on a JSM-5910 microscope operated at 20 kV using a secondary electron detector.

2.9. Dynamic light scattering

The 0.25 wt% starch solution was pushed through 0.45-μm filter (PTFE, Millipore UFC30LG25, America) and the 0.50-M $CuCl_2$ solution was pushed through a 0.1-μm filter (PTFE, Millipore UFC30LG25, America). Appropriate amounts of the two solutions were then mixed to yield solutions at r = 0.092, 0.70, and 1.41, respectively. Light scattering measurements were performed after the mixtures were heated at 70 °C for 30 min and then cooled down for 2 h to room temperature.

Dynamic light scattering measurements were performed at 25 °C on a Brookhaven 90Plus Particle Size Analyzer. The scattering angles used were 15° and 90°, respectively, and the light source used was a 35-mW diode laser. The size and polydispersity values were automatically generated by the instrument after each measurement.

3. Results and discussion

3.1. Amylose

The template used for CuS particle synthesis was amylose. Amylose, the linear portion of starch, consists of (1 → 4)-linked α-D-glucopyranosyl units (Scheme 1a). Amylose dissolves in water at temperatures above 60–70 °C and assumes essentially random-coil conformations (Brant & Dimpfl, 1970). Below 60–70 °C, amylose undergoes retrogradation involving chain alignment, crystallization, and eventual amylose precipitation (Gidley, 1989; Miles, Morris, Orford, & Ring, 1985). Our amylose stock solution at 0.25 wt% in water was produced by heating the mixture at 100 °C for 30 min and storing the solution at room temperature (25 ± 5 °C). Our observation revealed that the no noticeable precipitate was produced from this solution within 1 week after its preparation. Before the stock solution was used, it was always heated at 70 °C for 30 min again to ensure amylose dissolution.

The amylose used in this study was analyzed by size exclusion chromatography (SEC) at 40 °C using 0.1 M aqueous NaCl as the eluant. Based on poly(ethylene glycol) standards, the number-average molecular weight M_n and polydispersity index M_w/M_n were 1.22×10^4 g/mol and 2.27, respectively. Since amylose has a much higher hydrodynamic volume than that of PEG used for SEC column calibration, the M_n of amylose evaluated with SEC will be higher than the value expected for native amylose. However, in present study, the tested M_n was lower than the value expected, possibly due to the degradation of amylose during manufacture as judged by the fact that amylose had excellent resolubility at a relatively low temperature compared to that of its native sample.

Because of the use of poly(ethylene glycol) as the calibration standards, the molecular weight determined was inaccurate. Furthermore, amylose was not directly soluble in room temperature water. While a freshly heated sample was used for analysis and amylose retrogradation was slow at the used low concentration, the sample might still contain some cooling-induced aggregates. This further increased the uncertainty for the determined amylose molecular weight. Amylose was not better characterized because we suspected that varying the amylose molecular weight over a certain range should not affect its complexing behavior with Cu^{2+} or its structure-directing effect on CuS nanoparticle formation.

3.2. Amylose complexation with Cu^{2+}

The CuS/amylose particles were prepared in three steps. In step 1, $CuCl_2$ was added into an amylose stock solution at 0.25 wt% heated at 70 °C to form a Cu^{2+} and amylose complex. At sufficiently high r, the added Cu^{2+} caused amylose aggregation. The occurrence of these processes was confirmed by results from our conductivity, TEM, and DLS experiments.

The complexation between Cu^{2+} and amylose, which contains three hydroxyl groups per glucopyranosyl unit, should not be surprising because poly(vinyl alcohol) or PVA is a known efficient sorbent for Cu^{2+} and PVA binds Cu^{2+} due to the chelating of its hydroxyl groups with Cu^{2+} (Hojo, Shirai, & Hayashi, 1974). In fact, this complexion has been previously observed between Cu^{2+} and the hydroxyl groups of starch granules (Ciesielski & Tomasik, 2004) as well as between Cu^{2+} and the surface hydroxyl groups of suspended starch particles (Miao, Li, Deng, Wang, & Liu, 2010). While small-molecules such as 1,3-butanediol do not complex with Cu^{2+}, polymers bearing hydroxyl groups do probably because the hydroxyl groups in a polymer chain are close already and the formation of a complex in this case may lead to much less reduction in the system's entropy than when several small molecule alcohols are brought together to form a complex with Cu^{2+}.

Prior electron paramagnetic resonance and titration experiments suggested that the complex formed between Cu^{2+} and PVA was polynuclear with a structure shown in Scheme 1b below (Godard, Wertz, Biebuyck, & Mercier, 1989):

A similar complexion was suspected to occur between Cu^{2+} and the amylose hydroxyl groups. The four hydroxyl groups participating in the formation of one complex can be from the same amylose chain resulting in intra-chain complexation. If hydroxyl groups of different chains are involved in the formation of one complex, amylose aggregation is promoted by this inter-chain complexion.

Cu^{2+}-induced amylose aggregation was first confirmed by our DLS experiments. Cu^{2+} and the amylose stock solution at 0.25 wt% were mixed at r = 0.092, 0.70, and 1.41. The mixtures were then heated at 70 °C for 30 min and allowed to cool down to room temperature in 2 h before DLS analyses. The hydrodynamic diameter D_h of the amylose sample was 49 nm (Table 1), suggesting the existence of some amylose aggregates at room temperature aside from

Table 1
Comparison of DLS and TEM results for amylose and Cu^{2+}/amylose samples at different r values.

r	D_h (nm)	PDI	Team diameter (nm)
0	49	0.027	45 ± 8
0.092	49	0.026	25 ± 10
0.70	150	0.028	158 ± 22
1.41	252	0.030	282 ± 55

the molecularly dissolved amylose. The D_h value of the sample at $r = 0.092$ remained at 49 nm, suggesting that Cu^{2+} at this amount was incorporated into the existing amylose aggregates and single chains and was insufficient to induce further amylose aggregation. The D_h values increased to 150 and 252 nm at $r = 0.70$ and 1.41, respectively, suggesting that Cu^{2+} at these concentrations promoted amylose aggregation and this aggregation occurred most likely due to the bridging effect provided Cu^{2+} between different amylose molecules or aggregates.

This Cu^{2+}-promoted amylose aggregation was also confirmed by our TEM results. The afore-mentioned heated and cooled amylose and Cu^{2+}/amylose samples at $r = 0.092$, 0.70, and 1.41, respectively, were aero-sprayed or atomized on Formvar-coated copper grids. While the Cu^{2+}/amylose samples were not further stained before TEM analysis due to the presence of Cu^{2+} as an inherent stain, the sprayed and dried amylose sample was negatively stained by uranyl acetate. Fig. 1 compares TEM images of the different samples.

The TEM specimens were prepared by aero-spraying because this helped speed up solvent evaporation and minimize morphological changes of the particles during the solvent removing step. Using this specimen protocol, the atomized water spray evaporated ~3 s after its landing on a TEM grid. An aqueous uranyl acetate solution was used to stain the amylose sample because room-temperature did not dissolve amylose.

Three types of amylose aggregates were observed by TEM and they were spheres with an average diameter of 45 ± 8 nm, worms with an average diameter of 5 ± 2 nm, and smaller particles with an average diameter of 9 ± 2 nm. Since the diameter of the large spheres agreed with the D_h value of 49 nm determined from DLS, these large spheres probably existed in the solution phase already. We had no evidence suggesting the presence of these wormlike structures and smaller particles in the solution phase because they were not detected by DLS, a technique which was biased toward larger particles. At least two types of aggregation states were observed for Cu^{2+} in the Cu^{2+}/amylose sample $r = 0.092$. There were larger dark Cu^{2+}-rich domains with a diameter of around 35 nm and the smaller Cu^{2+}-rich domains with a diameter of about 5 nm. More interestingly, the smaller dots seemed to form lines and four of these were traced in the TEM image in Fig. 1b. Since our DLS results suggested that Cu^{2+} did not change the aggregation state of amylose at this small r value and Cu^{2+} incorporated into the existing amylose aggregates, the larger Cu^{2+}-rich domains must be the original large amylose aggregates now impregnated with Cu^{2+}. The lined little dots were probably formed due to the deposition of Cu^{2+} in regions of the original wormlike amylose structures.

At $r = 0.70$ and 1.41, particles much larger than those seen in Fig. 1a and b were observed, confirming Cu^{2+}-induced amylose aggregation. In Table 1 are compared the TEM and DLS diameters of these particles. The size of the particles determined from these two methods agreed reasonably well with one another, suggesting the existence of the particles observed by TEM in the solution state.

Complexation between Cu^{2+} and amylose was also confirmed by comparing the conductivities of amylose samples before and after Cu^{2+} addition. In these experiments, amylose glucose subunit concentration was fixed at 0.0148 M or 0 but the added $CuCl_2$ concentration was varied. The conductivities σ_0 of the $CuCl_2$ solutions and those σ of the $CuCl_2$/amylose solutions were measured. Furthermore, σ of the $CuCl_2$/amylose solutions were measured before and after the mixtures were heated at 70 °C for 30 min. Plotted in Fig. 2 are the σ/σ_0 values at the r values of 0.092, 0.70, and 1.41, respectively.

In the presence of amylose, the $CuCl_2$ conductivity decreased mainly because Cu^{2+} complexed with amylose and the complexed Cu^{2+} had a reduced mobility. More interestingly, the ratio σ/σ_0 experienced a further substantial decrease from ~0.90 to ~0.50 after Cu^{2+} and amylose were heated at 70 °C for 30 min. This suggested that the complexation was more favored at 70 °C than at room temperature. Since both free Cu^{2+} and Cl^- were to conduct electricity (Gizdavic-Nikolaidis, Travas-Sejdic, Cooney, & Bowmaker, 2006) and the counter Cl^- should not bind with the Cu^{2+}/amylose aggregates so tightly and should have contributed

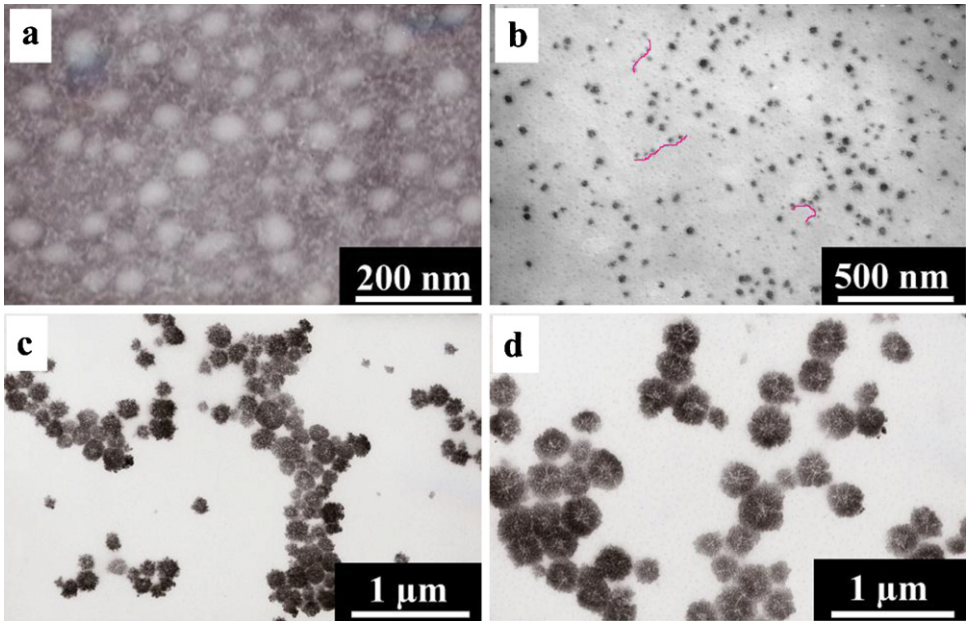

Fig. 1. TEM images of aero-sprayed samples of amylose (a) and Cu^{2+}/amylose at $r = 0.092$ (b), 0.7 (c), and 1.41 (d), respectively. The inserted red-lines in Fig. 1b are just guided for eyes. (For interpretation of the references to color in this figure legend, the reader is referred to the web version of this article.)

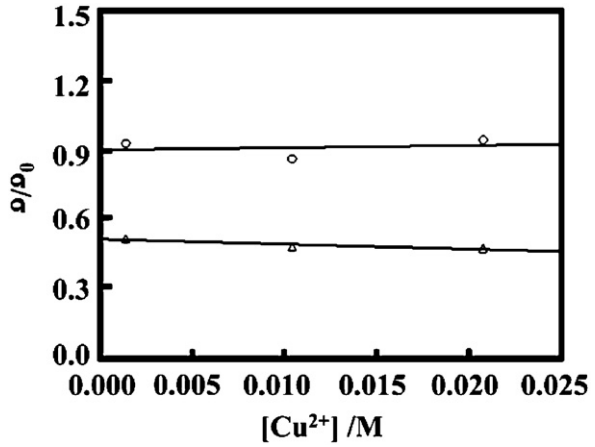

Fig. 2. Plot of conductivity ratios, σ/σ_0, between $CuCl_2$/amylose solutions and $CuCl_2$ solutions at different $CuCl_2$ concentrations before (o) and after (Δ) the $CuCl_2$/amylose solutions were heated at 70 °C for 30 min.

little to σ reduction, the observed small σ/σ_0 values suggested Cu^{2+} binding in high percentages after the mixture was heated at 70 °C. It should be pointed that conductivity measurement as demonstrated in present article, is an effective method for the evaluation of complexation between metal ions and amylose. This method might be extended for the system, for example, other minerals complexed with starch as evaluated by following conductivity variation (Behall, Howe, & Anderson, 2002).

3.3. CuS particle formation process

The subsequent steps in CuS@amylose particle synthesis were derived from the procedures proposed by Yamamoto et al. (1993) and Nagarathinam, Chen, et al. (2009) and Nagarathinam, Saravanan, et al. (2009). In step 2, the amylose-complexed Cu^{2+} was reacted with 1.5 Mequiv. of $Na_2S_2O_3$ at 70 °C for 2 h. According to Zhang, Qiao, and Hu (2004), this should initially lead to the precipitation of Cu^{2+} in the form of CuS_2O_3:

$$Cu^{2+} + S_2O_3{}^{2-} + 2H_2O \rightarrow [CuS_2O_3{\cdot}2H_2O] \downarrow \quad (1)$$

Over 2 h as demonstrated by Yamamoto et al. (1993). CuS_2O_3 disproportionated to yield CuS:

$$[CuS_2O_3{\cdot}2H_2O] \rightarrow CuS \downarrow + SO_4{}^{2-} + 2H^+ + H_2O \quad (2)$$

The CuS particles produced at 70 °C were amorphous. The particles prepared at $r = 1.41$ were hydrothermal synthesized in a sealed autoclave at 100 °C for 0, 3, 30, and 120 min as well as 24 h. After sample purification, drying, and redispersion in water by ultrasonication, the particles were aero-sprayed for TEM analysis. Fig. 3 shows TEM images of the samples taken at different hydrothermal times.

The composite microparticles shown in Fig. 3a were not hydrothermal prepared and bore much resemblance to the Cu^{2+}/amylose particles seen in Fig. 1d. A dynamic light scattering measurement revealed that the D_h value was 258 nm, which was close to 250 nm for the particles before $S_2O_3{}^{2-}$ addition. A closer scrutiny also revealed differences. The microspheres in Fig. 1d seemed to have a dark shell and a light core. The shells appeared uniformly dark except light streaks. The spheres in Fig. 3a did not have a clear

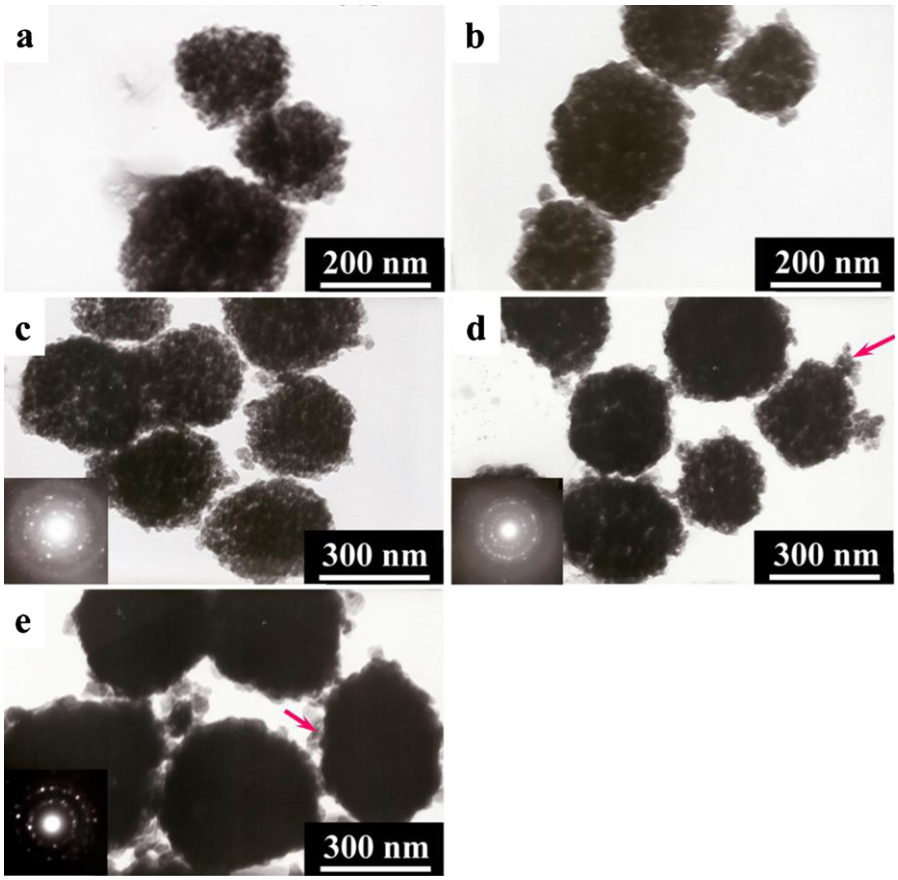

Fig. 3. TEM images of hierarchical CuS composite microspheres that were prepared at $r = 1.41$ and 70 °C and then hydrothermal synthesized at 100 °C for 0 min (a), 3 min (b), 30 min (c), 2 h (d), and 24 h (e), respectively. The insets are the corresponding area electron diffraction patterns.

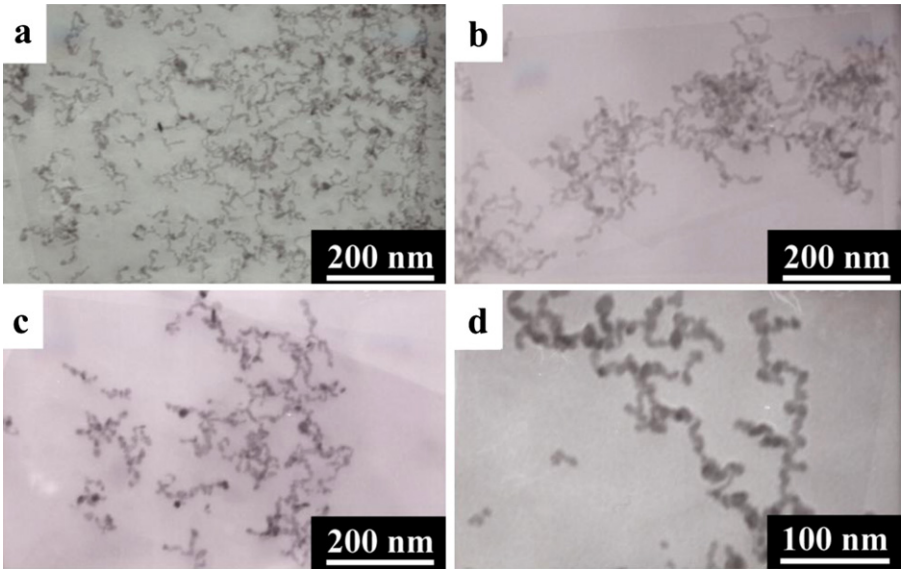

Fig. 4. TEM images of hierarchical CuS composite microspheres that were prepared at $r = 1.41$ and 70 °C and then hydrothermal synthesized at 100 °C for 0 min (a), 3 min (b), 30 min (c), 2 h (d), and 24 h (e), respectively. The insets are the corresponding area electron diffraction patterns.

core–shell structure but had more rugged surfaces and seemed to consist of fused dark and light nanodomains that did not possess a regular shape or a uniform size.

The spheres in Fig. 1d had approximately uniform shells because Cu^{2+} complexed with amylose and should be uniformly distributed inside amylose phase. The streaks might be cracks formed during TEM specimen preparation after solvent evaporation. The cores were light probably because the spheres were formed in the early stage of amylose aggregation and the Cu^{2+} added dropwise in the later stage had difficulty diffusing into the core.

Distinct light and dark nanodomains were seen in the composite microspheres of Fig. 3a but a core–shell structure was missing. The dark nanodomains must have corresponded to regions enriched with amorphous CuS nanoparticles. Since no covalent bonds existed between CuS and amylose, the segregation of the CuS nanoparticles formed from the amylose matrix should not be surprising. A clear lighter core in the microparticle center was not seen in this case probably because the sample was heated for another 2 h at 70 °C after $Na_2S_2O_3$ addition. The longer heating might have helped achieve a more uniform distribution over the entire microparticle (not over the nanometer scale) of the produced CuS nanoparticles.

The agreement because the D_h values of the microspheres before and after $Na_2S_2O_3$ addition suggested the synthesis of $CuS_2O_3{\cdot}2H_2O$ inside the original Cu^{2+}/amylose template. The template synthesis of $CuS_2O_3{\cdot}2H_2O$ should not be surprising because a high percentage of Cu^{2+} ions were complexed with amylose as deduced from our conductivity data and the precipitation reaction shown in Eq. (1) should occur predominantly in regions where Cu(II) was concentrated. Our speculation was that the complexed Cu(II) was in constant equilibrium with Cu^{2+} and the free Cu^{2+} reacted with $S_2O_3^{2-}$ to form a precipitate. The higher stability of CuS_2O_3 eventually favored the precipitate over the Cu^{2+}/amylose complex. The CuS_2O_3 precipitate decomposed over time at 70 °C into CuS.

The microparticles before hydrothermal synthesized (Fig. 3a) and those hydrothermal synthesized for 3 min at 100 °C possessed no area electron diffraction (SAED) patterns and was amorphous. It was only after 30 min annealing that a SAED pattern appeared, suggesting formation of a crystalline phase.

With further hydrothermal synthesizing, the microparticles got bigger as revealed by the TEM images shown in Fig. 3. We have also performed DLS analysis of samples hydrothermal synthesized for different times. The D_h values at the hydrothermal times of 0, 3, 30, and 120 min as well as 24 h were 258, 271, 280, 340, and 380 nm, respectively. The size increase must be caused by the Oswald ripening of the composite particles, which grew via the dissociation of the smaller composite particles and the incorporation of their fragments, some marked by arrows in Fig. 3d and e, into the larger composite particles.

The structural evolution of the particles prepared at $r = 0.092$ was also followed by TEM analysis of samples prepared using different hydrothermal times and Fig. 4 shows TEM images of some samples. The wormlike structure was seen throughout this process. Also, the structure seemed to thicken with hydrothermal time.

The hydrodynamic diameters of the samples at $t = 0$ and 24 h were determined by DLS to be 74 and 81 nm, respectively. Since we could not tell if worm fragmentation took place during this hydrothermal process, the D_h value increase could not be used as evidence for worm thickening.

We do not know the mechanism for the formation of the worm-like structures. If the worms seen in Fig. 1a did exist at 70 °C and these structures persisted after Cu^{2+} incorporation, the composite particles seen in Fig. 4a would be product of a template synthesis. The worms formed probably for the bundling of amylose chains. These small structures with high specific surface areas existed probably because not enough Cu^{2+} was added to induce worm–worm aggregation.

We did not follow the growth of the composite particles at $r = 0.70$ because these particles had morphologies similar to those prepared at $r = 1.41$ and their structural evolution process should be similar to that for the particles prepared at $r = 1.41$. The major difference was that the composite CuS@amylose particles prepared at $r = 0.70$ were smaller than those prepared at $r = 1.41$. This was also true for the Cu^{2+}/amylose particles prepared at the two r values.

3.4. CuS formation

CuS formation under our standard CuS@amylose particle preparation conditions involving hydrothermal synthesis of the initial

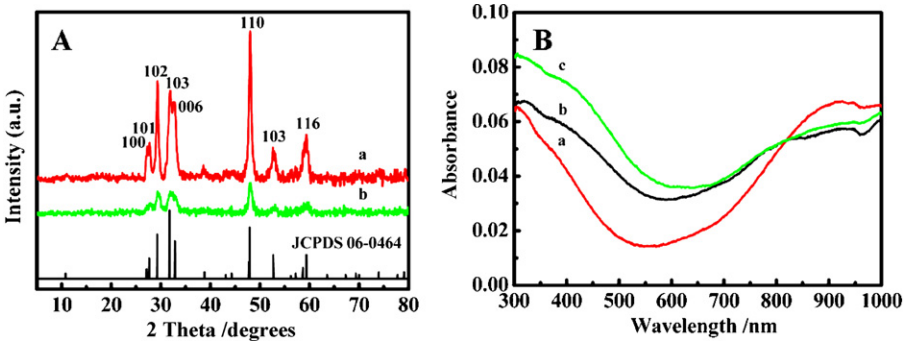

Fig. 5. (A) XRD patterns of CuS prepared at $r = 1.41$ (a) and $r = 0.092$ (b) as well as the bar graph for the hexagonal covellite phase (bottom); (B) comparison of UV–visible absorption spectra of CuS prepared at $r = 0.092$, 0.70, and 1.41, respectively.

crude product at 100 °C for 24 h was confirmed by our wide angle X-ray diffraction (XRD) study of the resultant particles. The particles after preparation were washed with ethanol and water, dried under vacuum, and then used for XRD. Fig. 5A compares XRD patterns of the particles prepared at $r = 0.092$ and 1.41 as well as the bar graph for the hexagonal CuS phase (JCPDS No. 06-0464) pattern. The agreement between the observed patterns and the bar graph confirmed the preparation of covellite under our conditions.

The vacuum-dried CuS@amylose particles were also ultrasonicated in distilled water and their absorption spectra were measured and shown in Fig. 5B. All the samples exhibited strong absorption at ~300 nm. Their absorption decreased with wavelength until ~600 nm and picked up again in the near IR region (Liu & Xue, 2011). These were all characteristic of CuS nanoparticles and further confirmed CuS preparation under our conditions.

3.5. Amylose-directed synthesis

CuS particles were also prepared under conditions identical to those used to prepare the CuS@amylose particles except the replacement of the amylose stock solution by water. Compared in Fig. 6a, b, d, e, g, and h are the TEM images of the particles prepared under the two sets of conditions.

When amylose was used, the morphology of the CuS@amylose particles changed from wormlike at $r = 0.092$ (Fig. 6b) to microspheres at $r = 0.70$ (Fig. 6e) and 1.42 (Fig. 6h). We have so far suggested that r changes were the cause for the morphological changes. In reality, the amylose concentration was maintained approximately constant in these experiments. The r changed as a result of $[Cu^{2+}]$ change. Thus, the corresponding control experiment for each r value involved the use of a different $[Cu^{2+}]$.

In the control experiment for $r = 0.092$, irregularly shaped particles involving elongated particles were produced as seen in Fig. 6a. Particles that were ~1 μm in size were seen in Fig. 6d and g, respectively. Also, elongated particles that seemed to have formed from sphere fusion were also seen in these images. Therefore, totally different CuS particles were produced without amylose. The amylose added had a morphology-directing effect.

SEM was also used to characterize the CuS@amylose particles and Fig. 6c, f, and i shows the resultant SEM images. The wormlike

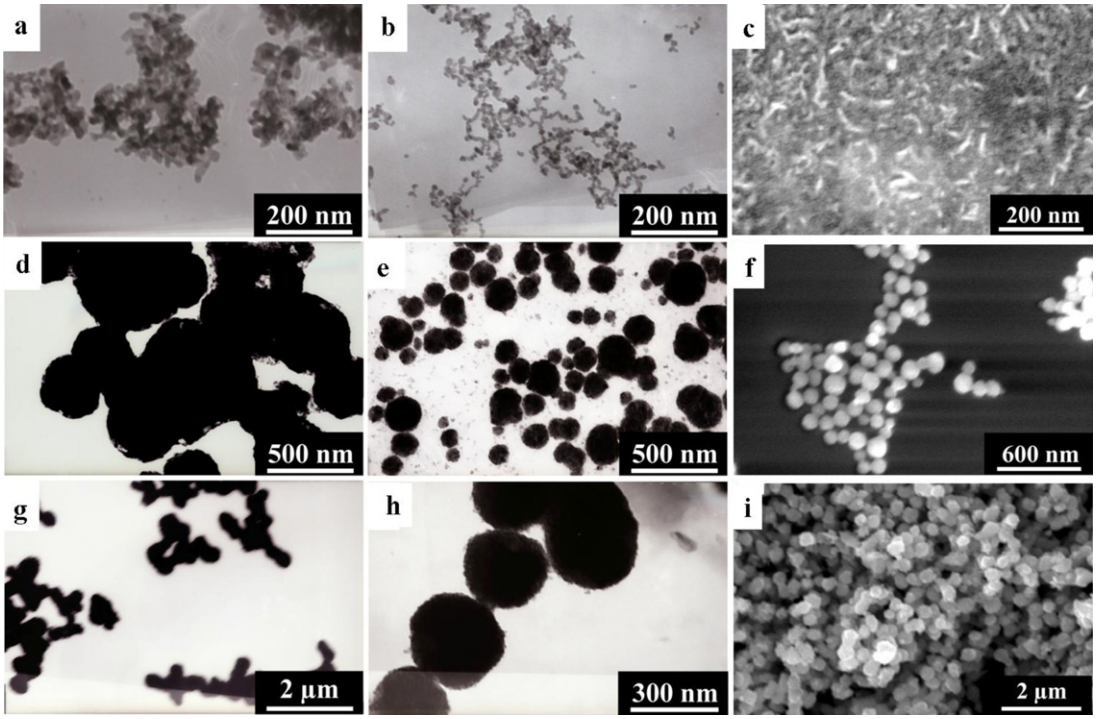

Fig. 6. TEM images of CuS prepared at the r values of 0.092 (b), 0.70 (e), and 1.41 (h). Also shown are the CuS particles prepared under otherwise identical conditions as those prepared at $r = 0.092$ (a), 0.70 (d), and 1.41 (g) but without using amylose, and SEM images of the CuS samples prepared at $r = 0.092$ (c), 0.70 (f), and 1.41 (i), respectively.

shape of the CuS@amylose particles prepared at $r = 0.092$ and the spherical shape of the particles prepared at $r = 0.70$ and 1.41 were clearly confirmed.

4. Conclusions

Cu^{2+} and amylose were complexed in water. This complexation was verified by a reduction in $CuCl_2$ conductivity after amylose addition. It also caused amylose to associate into different Cu^{2+}/amylose aggregates depending on r. At the low Cu^{2+} to α-D-glucopyranosyl unit molar ratio r of 0.092, the added Cu^{2+} did not perturb the aggregation state of the amylose as suggested by our DLS results. As r increased to 0.70 and 1.41, Cu^{2+} promoted the aggregation of amylose into microspheres with sizes around 150 and 250 nm, respectively. The addition of $Na_2S_2O_3$ at 70 °C led first to the precipitation of CuS_2O_3 and then the formation of amorphous CuS nanoparticles as a disproportionation product of CuS_2O_3 inside the original Cu^{2+}/amylose aggregates. Hydrothermal preparing at 100 °C eventually turned the amorphous CuS nanoparticles into crystalline particles. Thus, this resulted in the formation of crystalline CuS@amylose worms at $r = 0.092$ and crystalline CuS@amylose composite microspheres at $r = 0.70$ and 1.41. The composite particles were larger at $r = 1.41$. CuS formation was confirmed by XRD and UV–visible absorption results. Our control experiments indicated that these composite particles with interesting morphologies were formed only in the presence of amylose and thus suggested amylose-directed formation of these particles. Since the preparation procedures are simple and CuS has interesting optical and electric properties, this method may be used for producing CuS particles with unique morphologies for potential application in luminescence, lubrication, photo-catalysis, advanced battery, etc.

Acknowledgments

We thank financial support from the National Natural Science Foundation of China (Nos. 20474068 and 51173204), the Outstanding Overseas Chinese Scholars Funds of the Chinese Academy of Sciences, and the Leading Talents Program of Guangdong Province.

References

Basu, M., Sinha, A. K., Pradhan, M., Sarkar, S., Negishi, Y., & Govind Pal, T. (2010). Evolution of hierarchical hexagonal stacked plates of CuS from liquid–liquid interface and its photocatalytic application for oxidative degradation of different dyes under indoor lighting. *Environmental Science & Technology*, *44*(16), 6313–6318.

Behall, K. M., Howe, J. C., & Anderson, R. A. (2002). Apparent mineral retention is similar in control and hyperinsulinemic men after consumption of high amylose cornstarch. *Journal of Nutrition*, *132*(7), 1886–1891.

Brant, D. A., & Dimpfl, W. L. (1970). A theoretical interpretation of aqueous solution properties of amylose and its derivatives. *Macromolecules*, *3*(5), 655–664.

Buckel, W., & Hilsch, R. (1950). Zur supraleitung von kupfersulfid. *Zeitschrift Fur Physik*, *128*(2), 324–346.

Burton, L. C., & Windawi, H. M. (1976). Thermally induced changes of Cu_xS films and effect on CdS–Cu_xS solar-cell response. *Journal of Applied Physics*, *47*(10), 4621–4626.

Chairam, S., Poolperm, C., & Somsook, E. (2009). Starch vermicelli template-assisted synthesis of size/shape-controlled nanoparticles. *Carbohydrate Polymers*, *75*(4), 694–704.

Chang, P. R., Yu, J. G., Ma, X. F., & Anderson, D. P. (2011). Polysaccharides as stabilizers for the synthesis of magnetic nanoparticles. *Carbohydrate Polymers*, *83*(2), 640–644.

Chen, G. Y., Deng, B., Cai, G. B., Dong, W. F., Zhang, W. X., & Xu, A. W. (2008). Synthesis, characterization, and formation mechanism of copper sulfide-core/carbon-sheath cables by a simple hydrothermal route. *Crystal Growth & Design*, *8*(7), 2137–2143.

Chen, Y. B., Chen, L., & Wu, L. M. (2008). Water-induced thermolytic formation of homogeneous core–shell CuS microspheres and their shape retention on desulfurization. *Crystal Growth & Design*, *8*(8), 2736–2740.

Chung, J. S., & Sohn, H. J. (2002). Electrochemical behaviors of CuS as a cathode material for lithium secondary batteries. *Journal of Power Sources*, *108*(1–2), 226–231.

Ciesielski, W., & Tomasik, P. (2004). Complexes of amylose and amylopectins with multivalent metal salts. *Journal of Inorganic Biochemistry*, *98*(12), 2039–2051.

Cuevas, R. P., Gilbert, R. G., & Fitzgerald, M. A. (2010). Structural differences between hot-water-soluble and hot-water-insoluble fractions of starch in waxy rice (*Oryza sativa* L.). *Carbohydrate Polymers*, *81*(3), 524–532.

Ding, J. F., & Liu, G. J. (1999). Growth and morphology change of polystyrene-block-poly(2-cinnamoylethyl methacrylate) particles in solvent-nonsolvent mixtures before precipitation. *Macromolecules*, *32*(25), 8413–8420.

Folmer, J. C. W., & Jellinek, F. (1980). The valence of copper in sulfides and selenides—An X-ray photoelectron-spectroscopy study. *Journal of the Less-Common Metals*, *76*(1–2), 153–162.

Gao, J. N., Li, Q. S., Zhao, H. B., Li, L. S., Liu, C. L., Gong, Q. H., et al. (2008). One-pot synthesis of uniform Cu_2O and CuS hollow spheres and their optical limiting properties. *Chemistry of Materials*, *20*(19), 6263–6269.

Gidley, M. J. (1989). Molecular mechanisms underlying amylose aggregation and gelation. *Macromolecules*, *22*(1), 351–358.

Gizdavic-Nikolaidis, M., Travas-Sejdic, J., Cooney, R. P., & Bowmaker, G. A. (2006). Spectroscopic studies of interactions of polyaniline with some Cu(II) compounds. *Current Applied Physics*, *6*(3), 457–461.

Godard, P., Wertz, J. L., Biebuyck, J. J., & Mercier, J. P. (1989). Polyvinyl alcohol copper-II complex—Characterization and practical applications. *Polymer Engineering and Science*, *29*(2), 127–133.

Hall, R. B., Birkmire, R. W., Phillips, J. E., & Meakin, J. D. (1981). Thin-film polycrystalline Cu2s-Cd1-Xznxs solar-cells of 10-percent efficiency. *Applied Physics Letters*, *38*(11), 925–926.

Hojo, N., Shirai, H., & Hayashi, S. (1974). Complex-formation between polyvinylalcohol and metallic-ions in aqueous-solution. *Journal of Polymer Science Part C—Polymer Symposium*, (47), 299–307.

Hu, H. L., & Nair, P. K. (1996). Electrical and optical properties of poly(methyl methacrylate) sheets coated with chemically deposited CuS thin films. *Surface & Coatings Technology*, *81*(2–3), 183–189.

Johansson, J., Kostamo, J., Karppinen, M., & Niinistö, L. (2002). Growth of conductive copper sulfide thin films by atomic layer deposition. *Journal of Materials Chemistry*, *12*(4), 1022–1026.

Lee, H., Yoon, S. W., Kim, E. J., & Park, J. (2007). In situ growth of copper sulfide nanocrystals on multiwalled carbon nanotubes and their application as novel solar cell and amperometric glucose sensor materials. *Nano Letters*, *7*(3), 778–784.

Li, B. X., Xie, Y., & Xue, Y. (2007). Controllable synthesis of CuS nanostructures from self-assembled precursors with biomolecule assistance. *Journal of Physical Chemistry C*, *111*(33), 12181–12187.

Li, F., Wu, J., Qin, Q., Li, Z., & Huang, X. (2010). Controllable synthesis, optical and photocatalytic properties of CuS nanomaterials with hierarchical structures. *Powder Technology*, *198*(2), 267–274.

Liang, W., & Whangbo, M. H. (1993). Conductivity anisotropy and structural phase-transition in covellite CuS. *Solid State Communications*, *85*(5), 405–408.

Lindroos, S., Arnold, A., & Leskela, M. (2000). Growth of CuS thin films by the successive ionic layer adsorption and reaction method. *Applied Surface Science*, *158*(1–2), 75–80.

Liu, J., & Xue, D. (2010). Solvothermal synthesis of copper sulfide semiconductor micro/nanostructures. *Materials Research Bulletin*, *45*(3), 309–313.

Liu, J., & Xue, D. (2011). Rapid and scalable route to CuS biosensors: A microwave-assisted Cu-complex transformation into CuS nanotubes for ultrasensitive nonenzymatic glucose sensor. *Journal of Materials Chemistry*, *21*(1), 223–228.

Liufu, S. C., Chen, L. D., Yao, Q., & Huang, F. Q. (2008). In situ assembly of Cu_xS quantum-dots into thin film: A highly conductive p-type transparent film. *Journal of Physical Chemistry C*, *112*(32), 12085–12088.

Mao, J., Shu, Q., Wen, Y., Yuan, H., Xiao, D., & Choi, M. M. F. (2009). Facile fabrication of porous CuS nanotubes using well-aligned $[Cu(tu)]Cl{\cdot}1/2H_2O$ nanowire precursors as self-sacrificial templates. *Crystal Growth & Design*, *9*(6), 2546–2548.

Miao, Z., Li, Z., Deng, D., Wang, L., & Liu, Y. (2010). Novel crosslinked starch microspheres as adsorbents of Cu^{2+}. *Journal of Applied Polymer Science*, *115*(1), 487–490.

Miles, M. J., Morris, V. J., Orford, P. D., & Ring, S. G. (1985). The roles of amylose and amylopectin in the gelation and retrogradation of starch. *Carbohydrate Research*, *135*(2), 271–281.

Nagarathinam, M., Chen, J. L., & Vittal, J. J. (2009). From self-assembled Cu(II) coordination polymer to shape-controlled CuS nanocrystals. *Crystal Growth & Design*, *9*(5), 2457–2463.

Nagarathinam, M., Saravanan, K., Leong, W. L., Balaya, P., & Vittal, J. J. (2009). Hollow nanospheres and flowers of CuS from self-assembled Cu(II) coordination polymer and hydrogen-bonded complexes of N-(2-hydroxybenzyl)-L-serine. *Crystal Growth & Design*, *9*(10), 4461–4470.

Nair, P. K., Cardoso, J., Daza, O. G., & Nair, M. T. S. (2001). Polyethersulfone foils as stable transparent substrates for conductive copper sulfide thin film coatings. *Thin Solid Films*, *401*(1–2), 243–250.

Nozaki, H., Shibata, K., & Ohhashi, N. (1991). Metallic hole conduction in CuS. *Journal of Solid State Chemistry*, *91*(2), 306–311.

Ortega-Ojeda, F. E., Larsson, H., & Eliasson, A. C. (2004). Gel formation in mixtures of high amylopectin potato starch and potato starch. *Carbohydrate Polymers*, *56*(4), 505–514.

Roy, P., Mondal, K., & Srivastava, S. K. (2008). Synthesis of twinned CuS nanorods by a simple wet chemical method. *Crystal Growth & Design*, *8*(5), 1530–1534.

Sakamoto, T., Sunamura, H., Kawaura, H., Hasegawa, T., Nakayama, T., & Aono, M. (2003). Nanometer-scale switches using copper sulfide. *Applied Physics Letters*, *82*(18), 3032–3034.

Saunders, A. E., Ghezelbash, A., Smilgies, D. M., Sigman, M. B., & Korgel, B. A. (2006). Columnar self-assembly of colloidal nanodisks. *Nano Letters*, *6*(12), 2959–2963.

Shen, X. P., Zhao, H., Shu, H. Q., Zhou, H., & Yuan, A. H. (2009). Self-assembly of CuS nanoflakes into flower-like microspheres: Synthesis and characterization. *Journal of Physics and Chemistry of Solids*, *70*(2), 422–427.

Vigneshwaran, N., Nachane, R. P., Balasubramanya, R. H., & Varadarajan, P. V. (2006). A novel one-pot 'green' synthesis of stable silver nanoparticles using soluble starch. *Carbohydrate Research*, *341*(12), 2012–2018.

Wang, L. H., Xu, C., Zou, D. B., Luo, H., & Ying, T. K. (2008). Synthesis of hierarchical CuS flower-like submicrospheres via an ionic liquid-assisted route. *Bulletin of Materials Science*, *31*(7), 931–935.

Westrum, E. F., Stolen, S., & Gronvold, F. (1987). Thermodynamics of copper sulfides. 2. Heat-capacity and thermodynamic properties of synthetic covellite, CuS, from 5-K to 780.5-K—Enthalpy of decomposition. *Journal of Chemical Thermodynamics*, *19*(11), 1199–1208.

Xu, H., Wang, W., & Zhu, W. (2006). Sonochemical synthesis of crystalline CuS nanoplates via an in situ template route. *Materials Letters*, *60*(17–18), 2203–2206.

Xu, K., & Ding, W. (2008). Controlled synthesis of spherical CuS hierarchical structures. *Materials Letters*, *62*(29), 4437–4439.

Xu, S., Wang, Q., Cheng, J. H., Meng, Q. H., & Jiao, Y. (2010). Preparation and characteristics of porous CuS microspheres consisted of polycrystalline nanoslices. *Powder Technology*, *199*(2), 139–143.

Xue, P. C., Lu, R., Li, D. M., Jin, M., Tan, C. H., Bao, C. Y., et al. (2004). Novel CuS nanofibers using organogel as a template: controlled by bingding sites. *Langmuir*, *20*(25), 11234–11239.

Yamamoto, T., Tanaka, K., Kubota, E., & Osakada, K. (1993). Deposition of copper sulfide on the surface of poly(ethylene-terephthalate) and poly(vinyl alcohol) films in the aqueous-solution to give electrically conductive films. *Chemistry of Materials*, *5*(9), 1352–1357.

Yu, X. L., Wang, Y., Chan, H. L. W., & Cao, C. B. (2009). Novel gas sensoring materials based on CuS hollow spheres. *Microporous and Mesoporous Materials*, *118*(1–3), 423–426.

Yuan, K. D., Wu, J. J., Liu, M. L., Zhang, L. L., Xu, F. F., Chen, L. D., et al. (2008). Fabrication and microstructure of p-type transparent conducting CuS thin film and its application in dye-sensitized solar cell. *Applied Physics Letters*, *93*(13), 132106(1)–(3).

Zhang, J., & Zhang, Z. (2008). Hydrothermal synthesis and optical properties of CuS nanoplates. *Materials Letters*, *62*(15), 2279–2281.

Zhang, Y. C., Qiao, T., & Hu, X. Y. (2004). A simple hydrothermal route to nanocrystalline CuS. *Journal of Crystal Growth*, *268*(1–2), 64–70.

Zhu, H., Wang, J., & Wu, D. (2009). Fast synthesis, formation mechanism, and control of shell thickness of CuS hollow spheres. *Inorganic Chemistry*, *48*(15), 7099–7104.